



Conformation Dependence of Photophysical Properties of σ - π Conjugation as Demonstrated by *cis*- and *trans*-1,2-Diaryl-1,2-disilacyclohexane Cyclic Systems

Hayato Tsuji,* Yuki Shibano, Tohru Takahashi,[#] Makoto Kumada,[#] and Kohei Tamao*

International Research Center for Elements Science (IRCELS), Institute for Chemical Research, Kyoto University, Uji, Kyoto 611-0011

Received February 22, 2005; E-mail: tamao@scl.kyoto-u.ac.jp

Several configurationally constrained *cis*- and *trans*-1,2-diaryl-1,2-dimethyl-1,2-disilacyclohexanes (**3a–e**) have been synthesized in order to measure their photophysical properties, such as UV absorption, magnetic circular dichroism (MCD), and photoluminescence. As has been well established, the UV absorption maximum (1L_a band) occurs at 230–270 nm, due to the effective σ - π conjugation between the aryl groups and the disilane moiety. The absorption maximum wavelength of the *trans* isomer is slightly longer than that of the *cis* isomer for all the diaryldisilanes employed in the present study. Although the MCD spectra of the *cis*- and *trans*-1,2-diphenyl-1,2-dimethyl-1,2-disilacyclohexanes (**3a**) show only a slight configuration dependence, this method is helpful to detect a weak 1L_b band. The disilanes **3a** and **5a** show a charge-transfer (CT) emission band. The quantum yields are dependent on the disilane configuration and the solvent polarity; the order of the quantum yield is *cis*-**3a** < **5a** < *trans*-**3a** in 3-methylpentane, while the order is **5a** < *cis*-**3a** < *trans*-**3a** in acetonitrile. These results demonstrate that the conformation constraint is effective for controlling the photophysical properties of the diaryldisilanes.

It is well-known that the Si–Si σ -electron system possesses a high-lying HOMO and a low-lying LUMO. The energy level of a Si–Si σ -bonding orbital lies higher than that of a C=C π -orbital (e.g., the first ionization potential of Si₂Me₆: 8.69 eV;¹ benzene: 9.25 eV)² due to the inherent electropositivity of the silicon. Thus, the silicon σ -bonding electrons are labile to delocalize within the silicon framework similar to the π -conjugated system, and this σ -electron delocalization is called σ -conjugation. The Si–Si σ -conjugated system behaves as a chromophore in itself and exhibits intriguing photophysical properties, such as UV absorption and photoluminescence.^{3,4} At the same time, the strong interaction with the π -electron system affords a further electron-delocalized σ - π conjugation system, which has been well studied^{2b,5,6} due to the considerable interest from the viewpoints of basic science as well as material science.⁷ The most significant feature of the σ - π conjugation system is its remarkable stereoelectronic effect (conformation dependence). Kira, Sakurai, and their co-workers reported the UV absorption spectra of several conformation-constrained arylldisilanes and demonstrated that the torsion angle between the Si–Si σ -bond and the aromatic ring plane ω_1 (Fig. 1a) should be 90° for the maximum σ - π conjugation.⁸ In addition, much attention has been paid to the excited states of the σ - π conjugation system for elucidating the photo-physics and photochemistry of the aryl-substituted organo-silicon compounds.⁹

We have been carrying out the conformation control by the incorporation of a disilane moiety into a monocyclic¹⁰ or bicyclic^{11,12} system to clarify the relationship between the structure and photophysical properties of the oligosilane σ -conjugation system. Obviously, this methodology can also be applied to a

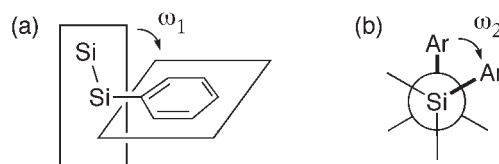


Fig. 1. (a) ω_1 : Torsion angle between the Si–Si σ -bonding axis and the aromatic ring plane; (b) ω_2 : torsion angle of C(ipso)–Si–Si–C(ipso).

diaryldisilane σ - π conjugation system. The photophysical properties of the diaryldisilanes are also postulated to depend on the torsion angle ω_2 , arising from the rotation around the Si–Si bond (Fig. 1), in addition to ω_1 as mentioned above. As shown in Fig. 2, these two angles can be constrained by means of the incorporation of the disilane moiety into a monocyclic structure to control the σ - π conjugation and the π - π interaction between the aromatic rings. In the present study, we have examined some photophysical properties, such as UV absorption, MCD (magnetic circular dichroism), and photoluminescence of the *cis*- and *trans*-1,2-diaryl-1,2-dimethyl-1,2-disilacyclohexanes.

Results and Discussion

Synthesis. The 1,2-diaryl-1,2-dimethyldisilacyclohexanes (**3a–e**) were prepared as summarized in Scheme 1, while their acyclic counterparts, the 1,2-diaryl-1,1,2,2-tetramethyldisilanes **5a–e**, are all known compounds.¹³ The reaction of the dichlorotetraphenyldisilane **1** with the di-Grignard reagent generated from 1,4-dichlorobutane afforded 1,1,2,2-tetraphenyl-1,2-disilacyclohexane **2**. One of the phenyl groups on each

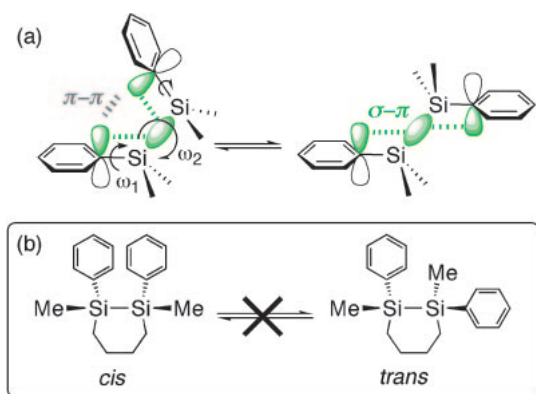
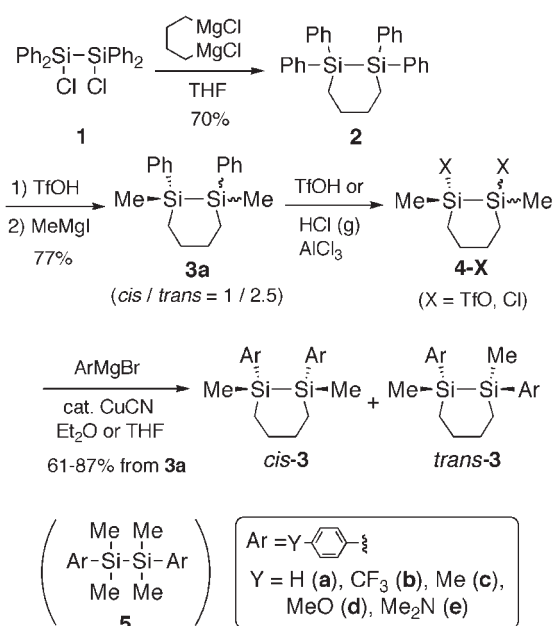


Fig. 2. (a) Schematic description of conformation change of acyclic 1,2-diphenyldisilane due to free rotation about Si–Si and Si–Ph bonds, and (b) conformationally constrained cyclic 1,2-diphenyldisilanes employed in this study.



Scheme 1.

silicon of **2** was substituted with trifluoromethylsulfonyloxy (TfO: triflate) groups,¹⁴ followed by the reaction with methylmagnesium iodide to give a mixture of the *cis*- and *trans*-1,2-dimethyl-1,2-diphenyl-1,2-disilacyclohexanes **3a**. The phenyl groups of the mixture of *cis*- and *trans*-**3a** were thoroughly substituted by chlorine atoms or triflate groups, followed by treatment with the corresponding aryl Grignard reagent in the presence of copper(I) cyanide¹⁵ to afford a mixture of the *cis*- and *trans*-disilanes **3b–e**. The two isomers of **3** were separated by flash column chromatography, preparative HPLC, or preparative GC.

The configuration of each isomer of **3a** was assigned according to the literature.¹⁶ In addition, the structure of *trans*-**3d** was unambiguously confirmed by X-ray crystallography (see below). These compounds **3a** and **3d** have characteristic ¹H NMR spectral patterns in the region of 0.8–2.2 ppm corresponding to the tetramethylene tethers. Thus, the eight protons

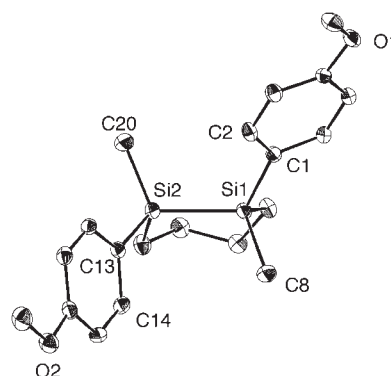


Fig. 3. X-ray structure of *trans*-**3d**. (ORTEP plot, 30% probability for thermal ellipsoids). Hydrogen atoms are omitted for clarity. Selected bond length, bond angles, and torsion angles: Si1–Si2: 2.3394(8) Å, C1–Si1–Si2: 115.90(6)°, C1–Si1–C8: 108.35(9)°, C13–Si2–Si1: 113.51(5)°, C13–Si2–C20: 109.64(9)°, C1–Si1–Si2–C13: –94.33(8)°, C8–Si1–Si2–C20: 154.52(12)°, Si2–Si1–C1–C2: 36.74(15)°, Si1–Si2–C13–C14: –69.19(15)°.

appear as three multiplets in the ratio of 2:2:4 from the low fields for the *trans* isomers, but in the ratio of 4:2:2 for the *cis* isomers. This difference was useful for the assignment of the *cis* and *trans* isomers of other derivatives.

Geometry. X-ray Crystallography: An X-ray crystallographic analysis was performed on the *trans* isomer **3d** (Fig. 3, Table 1). The Si–Si bond length and the Si–Si–C bond angles are within the normal range. The torsion angles, ω_1 , which primarily contribute to the degree of the σ – π conjugation, are 36.74(15)° and 69.19(15)°.

Geometry Optimization: The most probable geometries of **3a** and **5a** were obtained by MP2/6-311G(d) calculations, as shown in Fig. 4. The total energy of *trans*-**3a** is higher by only 0.94 kcal/mol than that of *cis*-**3a** at this level. The C(ipso)–Si–Si–C(ipso) torsion angles ω_2 of the *cis* and *trans* isomers are 34.6° and 167.1°, respectively. In the *cis*-isomer, the intramolecular distance between the two ipso-carbon atoms of the two phenyl groups (3.19 Å) is favorable for the intramolecular π – π interaction. The torsion angles ω_1 in the *cis* isomer are 63.1° and 70.0°, and those in the *C₂* symmetrical *trans* isomer are 56.6°, suggesting that the σ – π conjugation in the ground state is slightly more effective in the *cis* isomer. Actually, the HOMO energy level of *cis*-**3a** is slightly higher by 0.05 eV than that of *trans*-**3a** at the present level.

A conformation search by molecular mechanics calculations of the acyclic **5a** afforded the *gauche* and *anti* conformers as local minima. Further optimization with MP2/6-311G(d) calculations proved that the *gauche* conformer ($\omega_1 = 83.2^\circ$, $\omega_2 = 50.2^\circ$) is more stable¹⁷ than the *anti* conformer ($\omega_1 = 87.8^\circ$, $\omega_2 = 180^\circ$) by 1.8 kcal/mol. The torsion angles ω_1 are almost 90° in both conformers, suggesting the effective σ – π conjugation. The intramolecular distance between the two ipso-carbon atoms of the benzene rings in the *gauche* conformer is 3.51 Å, but the orbital overlap is not as large as that in *cis*-**3a**.

UV Absorption Spectra. The UV absorption spectra of **3** and **5** measured in 3-methylpentane at room temperature are plotted in Fig. 5 and the data are summarized in Table 2. The

Table 1. Crystal Data and Structure Refinement for *trans*-**3d**

Empirical formula	C ₂₀ H ₂₈ O ₂ Si ₂
Formula weight	356.60
Temperature	173(2) K
Wavelength	0.71070 Å
Crystal system	orthorhombic
Space group	<i>Pbca</i> (#61)
Unit cell dimensions	<i>a</i> = 8.0518(19) Å $\alpha = 90^\circ$ <i>b</i> = 17.507(4) Å $\beta = 90^\circ$ <i>c</i> = 28.671(7) Å $\gamma = 90^\circ$
Volume	4041.4(16) Å ³
Z	8
Density (calculated)	1.172 g/cm ³
Absorption coefficient	0.185 mm ⁻¹
<i>F</i> (000)	1536
Crystal size	0.50 × 0.30 × 0.10 mm ³
Theta range for data collection	3.16 to 27.48°
Index ranges	−10 ≤ <i>h</i> ≤ 9, −18 ≤ <i>k</i> ≤ 22, −37 ≤ <i>l</i> ≤ 37
Reflections collected	29947
Independent reflections	4629 [<i>R</i> (int) = 0.0361]
Completeness to theta = 27.48°	99.7%
Max. and min. transmission	0.9818 and 0.9134
Refinement method	Full-matrix least-squares on <i>F</i> ²
Data/restraints/parameters	4629/0/329
Goodness-of-fit on <i>F</i> ²	1.211
Final <i>R</i> indices [<i>I</i> > 2σ(<i>I</i>)]	<i>R</i> 1 = 0.0493, <i>wR</i> 2 = 0.1091
<i>R</i> indices (all data)	<i>R</i> 1 = 0.0521, <i>wR</i> 2 = 0.1107
Largest diff. peak and hole	0.297 and −0.184 e·Å ⁻³

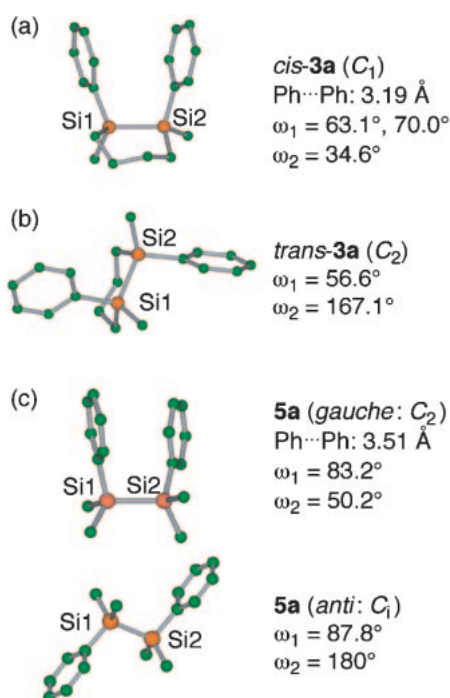


Fig. 4. Optimized geometries of (a) *cis*-**3a**, (b) *trans*-**3a**, and (c) **5a** at MP2/6-311G(d) level. Ph...Ph means the distance between the *ipso* carbon atoms on the phenyl rings.

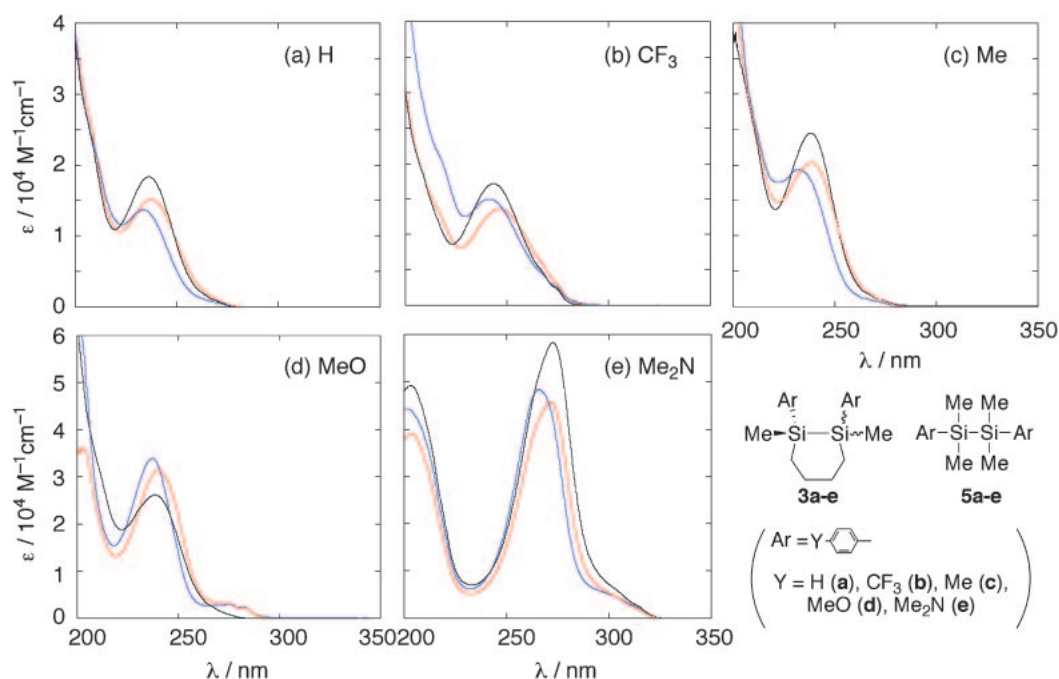
notable features of these spectra are as follows. (1) Substituent effects: The ¹*L*_a band of the parent compound **3a** is observed to red-shift in all the para-substituted derivatives **3b–3e**. The in-

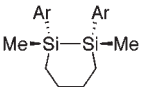
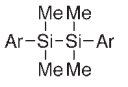
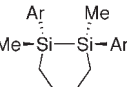
tensity of the ¹*L*_a band is increased by the electron-donating para-substituents such as methyl, methoxy, and dimethylamino groups, while it is decreased by the electron-withdrawing trifluoromethyl substituent. (2) Conformation effect: The absorption maximum wavelength λ_{\max} of the ¹*L*_a band red-shifts in the order of *cis*-**3a** < **5a** < *trans*-**3a**. Although the difference between the *cis* and *trans* isomers is only 4 nm (740 cm⁻¹, 0.09 eV), this tendency is always the case with the disilanes **3** employed in the present study. On the basis of the structural analysis (Fig. 4), a more efficient σ – π conjugation is expected in the *cis* isomer since the torsion angle ω_1 of *cis*-**3a** is larger than that of *trans*-**3a**. Therefore, the order of the UV absorption maximum wavelength would be *trans*-**3a** < *cis*-**3a**. However, the observed spectra disagree with this assumption. This discrepancy will be accounted for by the molecular orbital calculations and configuration interaction of the excited states on the basis of the time-dependent DFT calculations (see below).

(3) In addition to the intense ¹*L*_a band, weak absorption bands with a vibrational structure, assignable to the ¹*L*_b band of the aromatic rings, are observed at 250–315 nm for some compounds, especially ones with strong electron-donating or accepting groups such as the methoxy, *N,N*-dimethylamino, or trifluoromethyl groups. These bands were barely observable for the parent compounds **3a** and **5a** but their existence was unambiguously detected using MCD spectroscopy, as will be discussed later.

Molecular Orbital Calculations. To understand the electronic transitions of these disilanes, we carried out molecular orbital and excited state calculations.

Orbital Interaction: Figure 6a illustrates the molecular orbitals of the *cis*- and *trans*-**3a** drawn on the basis of the

Fig. 5. UV absorption spectra of *cis*-**3** (blue), *trans*-**3** (red), and **5** (black) in 3-methylpentane at room temperature.Table 2. Summary of UV Absorption Spectra of 1,2-Diaryldisilanes **3** and **5**^{a)}

		λ_{\max}/nm (ϵ)					
		 <i>cis</i> - 3a-e		 acyclic (5a-e)		 <i>trans</i> - 3a-e	
Y							
H	(a)	233.4 [234.6]	(13700) (13300) ^{b)}	236.4 [236.4]	(18400) (13300) ^{b)}	237.5 [238.0]	(15200) (14200) ^{b)}
CF ₃	(b)	241.1 268 (sh) ^{c)} 275 (sh) ^{c)}	(15000) (4300) (2400)	243.3 268 (sh) ^{c)} 275 (sh) ^{c)}	(17200) (4500) (2200)	246.7 268 (sh) ^{c)} 276 (sh) ^{c)}	(13600) (5600) (2500)
Me	(c)	232.0	(19300)	237.9	(24500)	238.6	(20700)
MeO	(d)	237.4 275.2 281.9	(33900) (3100) (2500)	238.6	(26200)	240.0 275.3 282.1	(31500) (3200) (2300)
Me ₂ N	(e)	266.1 305 (sh) ^{c)} 315 (sh) ^{c)}	(48300) (4200) (1900)	272.5 305 (sh) ^{c)} 315 (sh) ^{c)}	(58300) (5500) (2400)	271.4 305 (sh) ^{c)} 315 (sh) ^{c)}	(45600) (4200) (1800)

a) All measurements were performed in 3-methylpentane at room temperature unless otherwise noted. b) In acetonitrile at room temperature. c) Shoulder.

population analysis using the 6-311G(d) basis set. The HOMO is formed by the interaction between $\sigma(\text{SiSi})$ and $\pi_s(\text{Ph})$ and its energy level is significantly elevated compared with their levels. This interaction is consistent with the traditional description of the HOMO of an aryldisilane σ - π conjugated system.⁸ The LUMO is composed of the $\pi_s^*(\text{Ph})$ orbital and one of the originally degenerate π -symmetry orbitals with respect to the Si-Si bond ($\pi^*(\text{SiSi})$)¹⁸ rather than the Si-Si antibonding $\sigma^*(\text{SiSi})$, as illustrated in Fig. 6a and schematically drawn in Fig. 7. This is because the $\pi^*(\text{SiSi})$ orbital lies lower in energy than the $\sigma^*(\text{SiSi})$ orbital, as discussed in our previous report,^{1d} and the former is comparable in energy level to and thus interacts strongly with the $\pi^*(\text{Ph})$ orbitals. It is additionally

noted that the LUMO and LUMO+2 of *cis*-**3a** involve the interaction of two $\pi^*(\text{Ph})$ orbitals on the phenyl groups.

Orbital Energy: A key point in Fig. 6a is the comparison of the orbital energy levels. The HOMO energy level of *cis* is higher by 0.12 eV than that of the *trans*. This is consistent with the results from the geometry optimization calculations (Fig. 4), which claim that the σ - π interaction of the HOMO of *cis*-**3a** would be stronger than that of the *trans* due to the larger torsion angle ω_1 . However, the calculated HOMO-LUMO gaps of both isomers are essentially the same (5.64 eV for *cis* and 5.65 eV for *trans*). Since these analyses of the molecular orbitals did not provide useful information to elucidate the conformation dependence of the observed

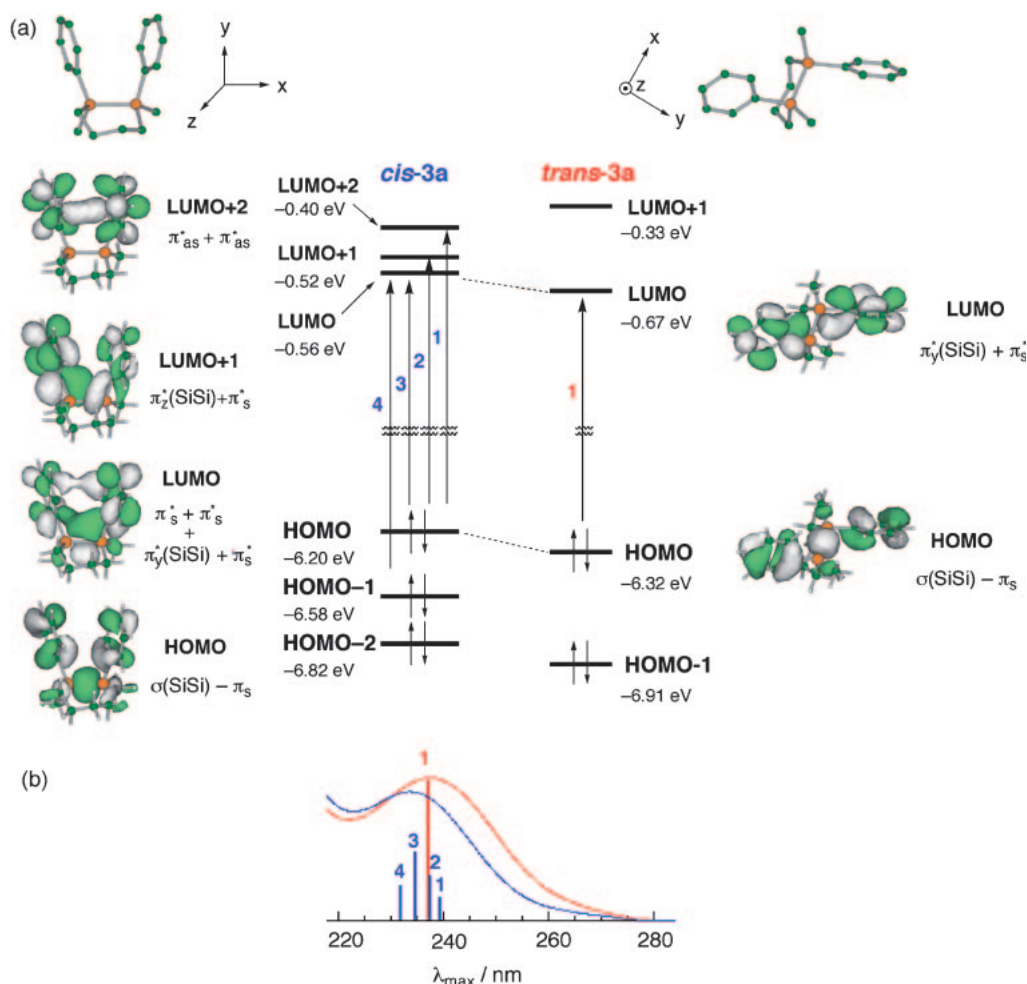


Fig. 6. Molecular orbitals of *cis*- and *trans*-3a drawn using 6-311G(d) basis set together with a simulation of the UV absorption spectra estimated by TD B3LYP/6-311G(d) calculations. The bars in the spectra represent the calculated transitions (shifted by 9.6 nm toward the short wavelength from the calculated values).

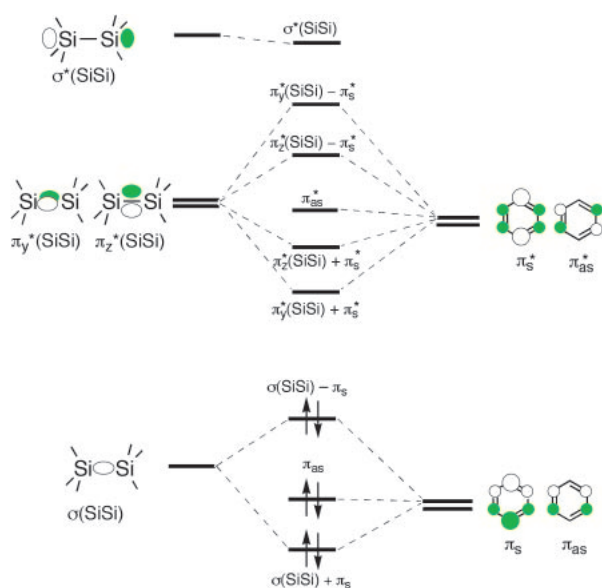


Fig. 7. Schematic drawing of some occupied and unoccupied molecular orbitals in a phenyl-substituted disilane.

UV absorption spectra, time-dependent DFT calculations were performed.

Excited State Calculations by the Time-Dependent DFT Method.

The results of the calculations (TD B3LYP/6-311G(d)//MP2/6-311G(d)) of the *cis*- and *trans*-3a as well as 5a are summarized in Table 3, in which some major transitions and excited configurations are highlighted with bold-face characters. The primary electronic transitions and the estimated UV spectra are visualized in Fig. 6b. Although the calculated excitation energies are somewhat underestimated, the observed spectra are reasonably reproduced. (1) For *trans*-3a, the observed 1L_a band is composed of only one transition ($S_0 \rightarrow S_1$) in which the excited configuration of HOMO \rightarrow LUMO is predominant. (2) In contrast, for *cis*-3a, the 1L_a band comprises four transitions with comparable excitation energies due to the congested molecular orbitals around the HOMO and LUMO. The most intense transition ($S_0 \rightarrow S_3$) is chiefly composed of the excited configuration of HOMO \rightarrow LUMO, but the higher-energy excited configurations also significantly participate in the transition, as shown in Table 3. As a result, the $S_0 \rightarrow S_3$ transition energy of the *cis* isomer becomes higher than that of the $S_0 \rightarrow S_1$ transition of the *trans*, and the UV

Table 3. Summary of the Time-Dependent DFT Calculations (TD B3LYP/6-311G(d)) for *cis*- and *trans*-**3a** and **5a**

<i>cis</i> - 3a (C_1 symmetry)	<i>trans</i> - 3a (C_2 symmetry)	<i>gauche</i> - 5a (C_2 symmetry)	<i>anti</i> - 5a (C_i symmetry)
S_1 (A) ^a : 249.05 nm ($f = 0.0162$) ^b	S_1 (B): 247.09 nm ($f = 0.2681$)	S_1 (A): 248.22 nm ($f = 0.0592$)	S_1 (A_u): 252.31 nm ($f = 0.5161$)
HOMO – 3 → LUMO ^c 0.16179 ^c	HOMO – 4 → LUMO 0.12121	HOMO – 3 → LUMO –0.13624	HOMO → LUMO 0.67392
HOMO – 2 → LUMO + 1 –0.13612	HOMO → LUMO 0.66877	HOMO – 2 → LUMO + 1 0.18144	S_2 (A_u): 245.90 nm ($f = 0.0000$)
HOMO – 1 → LUMO –0.10132	S_2 (B): 241.44 nm ($f = 0.0074$)	HOMO – 1 → LUMO + 1 –0.14863	
HOMO – 1 → LUMO + 1 –0.22694		HOMO → LUMO 0.57255	
HOMO → LUMO –0.24900	HOMO – 3 → LUMO + 1 –0.25749	HOMO → LUMO + 2 –0.28264	HOMO – 3 → LUMO + 3 0.16398
HOMO → LUMO + 1 0.28969	HOMO – 2 → LUMO 0.33289	S_2 (B): 247.82 nm ($f = 0.0107$)	HOMO – 2 → LUMO 0.33369
HOMO → LUMO + 2 0.47301	HOMO – 1 → LUMO + 3 –0.20810		HOMO – 1 → LUMO + 2 –0.20743
S_2 (A): 247.12 nm ($f = 0.0610$)	HOMO → LUMO + 2 0.51847		HOMO → LUMO + 1 0.56986
	S_3 (A): 241.11 nm ($f = 0.0000$)	HOMO – 3 → LUMO + 1 0.14224	S_3 (A_g): 244.51 nm ($f = 0.0000$)
		HOMO – 2 → LUMO + 2 –0.22261	
HOMO – 1 → LUMO –0.14587		HOMO – 1 → LUMO 0.51460	HOMO – 3 → LUMO + 1 0.18052
HOMO – 1 → LUMO + 1 0.17637	HOMO – 3 → LUMO –0.32833	HOMO → LUMO + 1 0.33540	HOMO – 2 → LUMO + 2 –0.21803
HOMO → LUMO –0.19650	HOMO – 2 → LUMO + 1 0.26162	HOMO → LUMO + 3 0.21974	HOMO – 1 → LUMO 0.36046
HOMO → LUMO + 1 0.49539	HOMO – 1 → LUMO + 2 –0.21259	S_3 (A): 242.69 nm ($f = 0.0586$)	HOMO → LUMO + 3 0.54492
HOMO → LUMO + 2 –0.34295	HOMO → LUMO + 1 –0.22900		
S_3 (A): 244.21 nm ($f = 0.1135$)	HOMO → LUMO + 3 0.46422		
	S_4 (B): 238.75 nm ($f = 0.0961$)	HOMO – 3 → LUMO 0.16869	
		HOMO – 1 → LUMO + 1 0.28323	
HOMO – 2 → LUMO + 2 –0.10065		HOMO – 1 → LUMO + 3 –0.16951	
HOMO – 1 → LUMO –0.17283		HOMO → LUMO 0.34948	
HOMO → LUMO 0.57987		HOMO → LUMO + 2 0.46481	
HOMO → LUMO + 1 0.22301			
HOMO → LUMO + 3 0.10387			
S_4 (A): 241.67 nm ($f = 0.0395$)		HOMO – 2 → LUMO 0.12752	
		HOMO – 2 → LUMO + 2 0.14954	
		HOMO – 1 → LUMO –0.24041	
HOMO – 3 → LUMO + 1 –0.19704		HOMO → LUMO + 1 0.59041	
HOMO – 2 → LUMO 0.12741		HOMO → LUMO + 3 –0.16119	
HOMO – 2 → LUMO + 2 0.26460			
HOMO – 1 → LUMO 0.41781			
HOMO → LUMO 0.11529			
HOMO → LUMO + 1 0.29091			
HOMO → LUMO + 3 –0.28667			

a) Irreducible representation to which each excited state belongs. b) Oscillator strength. c) Excited electron configurations. d) Coefficients of the wavefunction for each excitation.

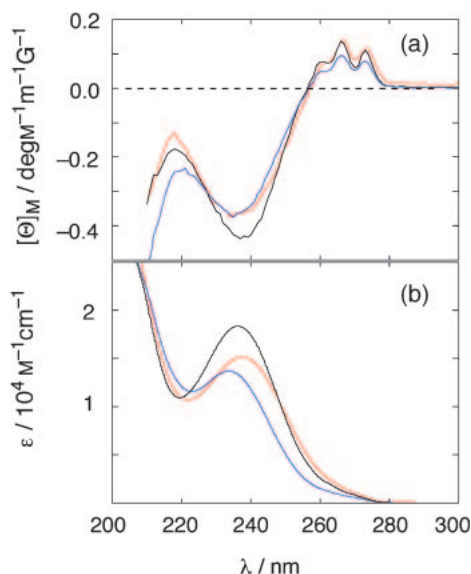


Fig. 8. (a) MCD spectra of *cis*-3a (blue), *trans*-3a (red), and 5a (black) measured in 3-methylpentane at room temperature, together with (b) the corresponding UV absorption spectra.

absorption maximum of *cis*-3a blue-shifts as compared to that of *trans*-3a. (3) The above mentioned conformation dependence of the UV absorption is the case for each conformer of the free-chain diphenyldisilane 5a. Thus, as shown in Table 3, the *gauche* conformer has four transitions in the corresponding region, including the most intense transition at 238.75 nm, which is shorter than that of *cis*-3a, while the *anti* conformer has only one transition at 252.31 nm, which is longer than that of *trans*-3a, with a much larger oscillator strength. The real spectrum of 5a is represented as a summation of these transitions, and the apparent peak happens to appear between those of the *cis*- and *trans*-3a.

MCD Spectroscopy. The magnetic circular dichroism (MCD) spectra of the *cis*- and *trans*-3a as well as 5a were observed in 3-methylpentane at room temperature. The spectra are plotted in Fig. 8 and the data are summarized in Table 4. The wavelength of the negative MCD peak (positive *B* term) at 234–237 nm coincides with that of the UV absorption maximum (1L_a band) of each compound. In addition, another band with a positive MCD signal (negative *B* term) was detected in the range of 260–273 nm with the vibrational fine structure of ca. 960 cm^{-1} and was assigned to the 1L_b band corresponding to the $\pi-\pi^*$ ($^1A_{1g} \rightarrow ^1B_{2u}$) transition in a benzene ring. Since the effect of the disilane moiety is slight on this transition, the shapes of the 1L_b band are essentially the same among these three spectra. These MCD signal patterns (i.e., positive for 1L_b and negative for 1L_a) observed in the present study are the same as those of phenylpentamethyldisilane¹⁹ and other silyl-substituted benzenes.²⁰

Photoluminescence. The emission spectra of the *cis*- and *trans*-3a and 5a excited at 250 nm were recorded at room temperature in 3-methylpentane and acetonitrile, as plotted in Fig. 9, and the data are summarized in Table 4. Several characteristic aspects are noted as follows. (1) Only one broad structureless emission band with a large Stokes shift was ob-

Table 4. Summary of MCD and Photoluminescence of the 1,2-Diphenyldisilanes *cis*-3a, *trans*-3a, and 5a^{a)}

	$\lambda_{\text{MCD}}^{\text{b)}}$ /nm([Θ] _M ^{c)}	$\lambda_{\text{EM}}^{\text{d)}}$ /nm ($\Phi^{\text{e)}}$ /10 ⁻³)	
		3-MP ^{f)}	CH ₃ CN
<i>cis</i> -3a	235 (−0.37)	366 (0.63)	387 (7.8)
	261 (0.05)		
	266 (0.10)		
	273 (0.08)		
<i>trans</i> -3a	234 (−0.37)	366 (3.9)	387 (9.5)
	261 (0.08)		
	267 (0.14)		
	273 (0.11)		
5a	237 (−0.44)	364 (1.4)	375 (3.7)
	261 (0.14)		
	266 (0.08)		
	273 (0.11)		

a) All spectra were recorded at room temperature. b) Maximum/minimum wavelength of MCD signal in 3-methylpentane. c) Magnetic molar ellipticity in a unit of $\text{deg M}^{-1} \text{m}^{-1} \text{G}^{-1}$. d) Emission maximum wavelength excited at 250 nm. e) Emission quantum yield. Naphthalene was used as a reference ($\Phi = 0.23$). f) 3-Methylpentane.

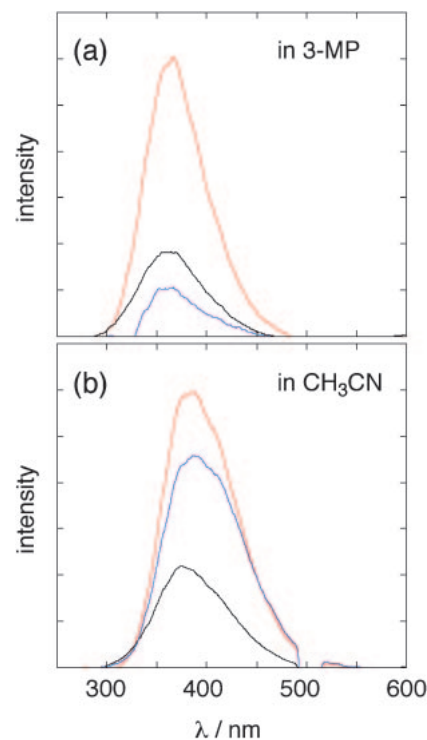


Fig. 9. Emission spectra of *cis*-3a (blue), *trans*-3a (red), and 5a (black) at room temperature: (a) in 3-methylpentane; (b) in acetonitrile.

served in both solvents. (2) The emission maximum wavelength, λ_{EM} , and the intensity depend on the polarity of the solvent. In acetonitrile, the λ_{EM} red-shifts by ca. 20 nm with an increase in intensity compared with that in 3-methylpentane. These facts demonstrate that the observed emission is that from the intramolecular charge-transfer (ICT) state, as has been developed by Shizuka, Ishikawa, Kumada et al.²¹

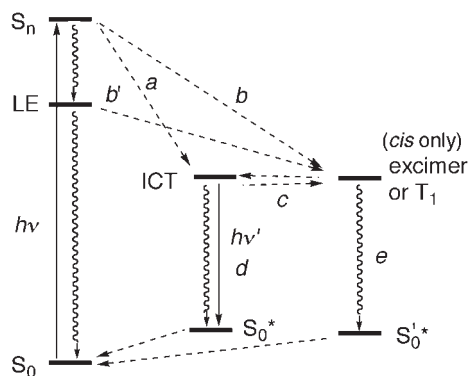


Fig. 10. Schematic energy levels of the ground and the excited states and relaxation paths for diaryldisilanes.

and Sakurai, Kira et al.²² (3) The 20 nm red-shift of λ_{EM} of **3a** and **5a** by changing the solvent from 3-methylpentane to acetonitrile is smaller than that (ca. 33 nm from isoctane to acetonitrile)^{22a} of pentamethylphenyldisilane. This can be understood by the less polar ICT states of the 1,2-diphenyldisilanes **3a** and **5a** due to the larger charge delocalization as compared to the monophenyldisilane. (4) The emission intensity is also dependent on the conformation. The orders of the emission quantum yield are *cis*-**3a** < **5a** < *trans*-**3a** in 3-methylpentane and **5a** < *cis*-**3a** < *trans*-**3a** in acetonitrile. The emission quantum yield of *trans*-**3a** is higher than those of the others in both solvents although the absolute values are low, while that of *cis*-**3a** is quite low in 3-methylpentane.

The conformation dependence of the emission intensity is explained in terms of the schematic diagram shown in Fig. 10. (i) The formation of the ICT state from the non-relaxed excited states S_n (path a)^{21g} followed by the radiative decay (path d) is more preferred in *trans*-**3a**, mainly due to steric reasons. (ii) The weak emission of the *cis*-**3a** in a non-polar solvent should be ascribed to another radiationless decay path. One possibility is the excimer formation (path b or b') or energy transfer on the basis of the intramolecular π - π interaction of the two phenyl groups in a non-polar solvent as seen in the calculated orbitals (Fig. 6a). However, the excimer in the *cis* isomer, even if really formed, would end up as a radiationless decay (e.g., path e) under the present conditions, because the band shape of *cis*-**3a** is the same as that of *trans*-**3a**, therefore, there is no significant distortion in the observed spectrum arising from the overlap with the excimer emission. There is another possibility that the intersystem crossing to the triplet state (path c)^{21c} would be more favored in the *cis* isomer. In any case, the formation of the polar ICT state is more preferred in acetonitrile to afford the CT emission with the larger quantum yield than that in 3-methylpentane. (iii) The emission quantum yield of the acyclic disilane **5a** is lower than those of the cyclic disilanes **3a** even in acetonitrile. Even considering the conformation change by varying the solvent, the relative quantum yield **5a** is too small. Therefore, this phenomenon can be attributable to another radiationless decay path, most probably due to the free rotation about the Si-Si bond. This result provides a nice example that demonstrates that the conformation constraint by the cyclic structure is effective for controlling the photophysical properties, especially the emission of the σ - π conjugation system.

Conclusion

A series of conformationally constrained *cis*- and *trans*-1,2-diaryl-1,2-disilacyclohexanes **3**, as well as their acyclic analogues **5**, have been prepared in order to investigate the effect of the conformation on their photophysical properties. (1) The UV absorption maximum wavelength of the *trans* isomer is always slightly longer (3–6 nm) than that of the *cis* isomer. (2) The 1L_a band in the MCD spectra is also conformation-dependent, while the first transition (1L_b band) is not. (3) The emission quantum yields, but not λ_{EM} , are significantly dependent on the conformation and solvent. The orders of the emission quantum yield are *cis*-**3a** < **5a** < *trans*-**3a** in 3-methylpentane and **5a** < *cis*-**3a** < *trans*-**3a** in acetonitrile. The conformation control by introduction of a cyclic structure is effective for controlling the photophysical properties in the σ - π conjugation system.

Experimental

General. Melting points (mp) were determined with a Yanaco MP-S3 instrument and are uncorrected. ^1H NMR spectra were measured with Varian Mercury (300 MHz for ^1H) in C_6D_6 . ^{13}C , ^{19}F , and ^{29}Si NMR spectra were measured with JEOL EX-270 (67.94 MHz for ^{13}C , 254.2 MHz for ^{19}F , and 53.67 MHz for ^{29}Si) spectrometer in C_6D_6 . Chemical shifts are reported in δ ppm with reference to internal solvent peak for ^1H (C_6HD_5 : 7.20 ppm) and ^{13}C (C_6D_6 : 128.0 ppm), to external CFCl_3 (0.0 ppm) for ^{19}F , and to external TMS (0.0 ppm) for ^{29}Si , respectively. Mass spectra were measured with SHIMADZU GCMS-QP5050 mass spectrometer. Recycle preparative gel permeation chromatography (GPC) was performed using polystyrene gel columns (JAIGEL 1H and 2H, LC-918, Japan Analytical Industry) with chloroform or toluene as an eluent. Recycle preparative high-performance liquid chromatography (HPLC) was performed using a silica-gel column (JAIGEL-SIL S-043-15, Japan Analytical Industry) or an ODS column (JAIGEL-ODS S-343-15 or JAIGEL-ODS-AP, Japan Analytical Industry). Preparative gas chromatography (GC) was performed using a silicone column (Silicone DC-550, 3 m \times 5 mm; column, injector, and detector temperature was 250 $^\circ\text{C}$; flow rate = 1.2 mL/s, hydrogen as a carrier gas; GC-4B, SHIMADZU). Thin-layer chromatography (TLC) was performed on plates coated with 0.25 mm thickness of silica gel 60F-254 (Merck). Column chromatography was performed by using Kieselgel 60 (70–230 mesh; Merck). All reactions were carried out under a nitrogen atmosphere, unless otherwise stated. All dry solvents were freshly distilled under N_2 before use. Et_2O and THF were distilled from sodium/benzophenone. Benzene was distilled from lithium aluminum hydride or sodium. Hexane was distilled from sodium/benzophenone/triglym. Toluene was distilled from sodium. CH_2Cl_2 was distilled from calcium hydride. Acetone was distilled from anhydrous K_2CO_3 .

Spectral Measurements. UV absorption spectra were recorded with a SHIMADZU UV-3101 spectrometer or a Perkin-Elmer Lambda 900 with a data interval of 0.1 nm. MCD spectra were recorded with a JASCO J-820 spectrometer in the presence of 1.5 T of magnetic field parallel to the propagation direction of the light (100 scans taken at 5 nm/min with 4 s response time were averaged). These spectra were taken with about 10^{-5} M solutions in a quartz cell with the path-length of 1 cm. Fluorescence spectra were recorded with a Perkin-Elmer LS50B spectrometer with a data interval of 0.5 nm. These spectra were taken with about

10^{-5} M solutions in a quartz cell with path-length of 1 cm. The fluorescence quantum yields were determined by comparison with a naphthalene as a standard ($\Phi = 0.23$ in cyclohexane).²³ 3-Methylpentane (3-MP) was purified by passage over a silver nitrate–alumina column and was degassed before the fluorescence measurement. Spectral grade acetonitrile was purchased (Nakalai Tesque) and degassed before use.

1,2-Dimethyl-1,2-diphenyl-1,2-disilacyclohexane (3a). To a solution of 1,1,2,2-tetraphenyl-1,2-disilacyclohexane (23.8 g, 56.7 mmol) in CH_2Cl_2 (100 mL) was added TFOH (10 mL, 110 mmol) dropwise at 0°C over 10 minutes. Upon completion of the addition, the addition funnel was rinsed with CH_2Cl_2 (2×2 mL). After being stirred at 0°C for 1.5 h, the solvent was evaporated. The residue was dissolved in Et_2O (100 mL) and cooled to 0°C . To the resulting solution was added 180 mL (170 mmol) of a 0.94 M solution of MeMgI in Et_2O dropwise at 0°C over 1.5 h. Upon completion of the addition, the addition funnel was rinsed with Et_2O (10 mL), then the reaction mixture was allowed to warm to room temperature. After being stirred for 1.5 h, the reaction mixture was hydrolyzed with 10% NH_4Cl (100 mL). Then the biphasic mixture was separated and the aqueous layer was extracted with Et_2O (3×100 mL). The combined organic layer was washed with brine (100 mL) and dried over MgSO_4 . After filtration and evaporation, the residue was subjected to silica-gel column chromatography (hexane, $R_f = 0.29$). The collected fraction was concentrated to give 12.9 g (43.6 mmol, 77% yield, *cis/trans* = 1/2.5) of 1,2-dimethyl-1,2-diphenyl-1,2-disilacyclohexane **3a** as a colorless oil.¹⁶

Isomers were separated by preparative HPLC (ODS, CH_3CN as eluent). *trans*-**3a**: ^1H NMR δ 0.38 (s, 6H), 1.08 (m, 4H), 1.59 (m, 2H), 1.96 (m, 2H), 7.2–7.3 (m, 6H), 7.55 (dd, $J = 7.4, 2.0$ Hz, 4H). ^{13}C NMR δ –4.55, 15.79, 26.54, 128.23, 128.94, 134.47, 138.48. ^{29}Si NMR δ –23.42. UV (λ_{max} (ϵ) in 3-MP) 237.5 (15200). UV (λ_{max} (ϵ) in acetonitrile) 238.0 nm (14200). *cis*-**3a**: ^1H NMR δ 0.42 (s, 6H), 0.9–1.0 (m, 2H), 1.15–1.25 (m, 2H), 1.7–1.85 (m, 4H), 7.15–7.2 (m, 6H), 7.4–7.5 (m, 4H). ^{13}C NMR δ –4.14, 15.89, 26.57, 128.05, 128.92, 134.80, 138.02. ^{29}Si NMR δ –23.37. UV (λ_{max} (ϵ) in 3-MP) 233.4 nm (13700). UV (λ_{max} (ϵ) in acetonitrile) 234.6 nm (13300).

Conversion from 3a to 3b–e. A Typical Procedure, 1,2-Dimethyl-1,2-bis(*p*-methylphenyl)-1,2-disilacyclohexane (3c): To a solution of 1,2-dimethyl-1,2-diphenyl-1,2-disilacyclohexane **3a** (1.04 g, 3.50 mmol) in CH_2Cl_2 (7 mL) was added TFOH (0.62 mL, 7.0 mmol) dropwise at 0°C to afford a mixture of *cis*- and *trans*-**4-OTf**. After being stirred for 1.5 h at 0°C , the solvent was evaporated. The crude **4-OTf** was dissolved in Et_2O (7 mL) and cooled to 0°C . To the resulting solution were added CuCN (31.7 mg, 0.354 mmol, 10.1 mol %) in one portion and 14.5 mL (14 mmol) of a 0.96 M solution of *p*-methylphenylmagnesium bromide in Et_2O dropwise over 10 min at 0°C . Upon completion of the addition, the addition funnel was rinsed with Et_2O (2 mL); then the reaction mixture was allowed to warm to room temperature. After being stirred for 1.5 h, the reaction mixture was hydrolyzed with 10% NH_4Cl (9 mL). The resulting biphasic mixture was separated and the aqueous layer was extracted with Et_2O (3×30 mL). The combined organic layer was washed with brine (50 mL) and dried over MgSO_4 . After filtration and evaporation, the residue was subjected to column chromatography on silica gel (hexane/AcOEt = 10/1, $R_f = 0.58$) followed by preparative HPLC (hexane/AcOEt = 20/1) to give 687 mg (2.12 mmol, 61% yield, *cis/trans* = 1/2.2) of 1,2-bis(*p*-methylphenyl)-1,2-dimethyl-1,2-disilacyclohexane **3c** as a colorless oil.

Isomers were separated by preparative GC. *trans*-**3c**: colorless crystals. mp $71\text{--}72^\circ\text{C}$. ^1H NMR δ 0.44 (s, 6H), 1.10–1.16 (m, 4H), 1.58–1.68 (m, 2H), 1.95–2.05 (m, 2H), 2.18 (s, 6H), 7.12 (d, $J = 7.8$ Hz, 4H), 7.53 (d, $J = 7.8$ Hz, 4H). ^{13}C NMR δ –4.37, 16.01, 21.58, 26.65, 129.10, 134.58, 134.86, 138.47. ^{29}Si NMR δ –23.67. MS (EI) m/z (relative intensity) 324 (M^+ , 11), 225 (100). UV (λ_{max} (ϵ) in 3-MP) 238.6 nm (20700). Found: C, 73.78; H, 8.75%. Calcd for $\text{C}_{20}\text{H}_{28}\text{Si}_2$: C, 74.00; H, 8.69%. *cis*-**3c**: a colorless oil. ^1H NMR δ 0.46 (s, 6H), 0.95–1.05 (m, 4H), 1.20–1.30 (m, 2H), 1.70–1.90 (m, 2H), 2.12 (s, 6H), 7.04 (d, $J = 7.7$ Hz, 4H), 7.46 (d, $J = 7.7$ Hz, 4H). ^{13}C NMR δ –3.92, 16.14, 21.55, 26.64, 128.95, 134.47, 134.93, 138.43. ^{29}Si NMR δ –23.67. MS (EI) m/z (relative intensity) 324 (M^+ , 13), 225 (100). UV (λ_{max} (ϵ) in 3-MP) 232.0 nm (19300). Found: C, 74.11; H, 8.89%. Calcd for $\text{C}_{20}\text{H}_{28}\text{Si}_2$: C, 74.00; H, 8.69%.

1,2-Dimethyl-1,2-bis(*p*-trifluoromethylphenyl)-1,2-disilacyclohexane (3b): Yield (67%, *cis/trans* = 1/2.6). Isomers were separated by preparative HPLC (ODS, CH_3CN as eluent). *trans*-**3b**: a colorless oil. ^1H NMR δ 0.20 (s, 6H), 0.90–0.96 (m, 4H), 1.44–1.58 (m, 2H), 1.80–1.94 (m, 2H), 7.32 (d, $J = 7.8$ Hz, 4H), 7.46 (d, $J = 7.8$ Hz, 4H). ^{13}C NMR δ –5.17, 15.13, 26.18, 124.71 (q, $J = 3.7$ Hz), 125.00 (q, $J = 271.7$ Hz), 131.03 (q, $J = 32.0$ Hz), 134.60, 143.12. ^{29}Si NMR δ –23.07. ^{19}F NMR δ –62.38. MS (EI) m/z (relative intensity) 432 (M^+ , 8), 314 (100). UV (λ_{max} (ϵ) in 3-MP) 246.7 nm (13600). Found: C, 55.37; H, 5.23%. Calcd for $\text{C}_{20}\text{H}_{22}\text{F}_6\text{Si}_2$: C, 55.53; H, 5.13%. *cis*-**3b**: a colorless oil. ^1H NMR δ 0.30 (s, 6H), 0.78–0.87 (m, 2H), 0.96–1.07 (m, 2H), 1.6–1.7 (m, 4H), 7.16 (d, $J = 8.3$ Hz, 4H), 7.32 (d, $J = 8.3$ Hz, 4H). ^{13}C NMR δ –4.71, 15.17, 26.24, 124.52 (q, $J = 3.7$ Hz), 124.90 (q, $J = 271.7$ Hz), 131.02 (q, $J = 32.0$ Hz), 134.80, 142.68. ^{29}Si NMR δ –22.82. ^{19}F NMR δ –62.42. MS (EI) m/z (relative intensity) 432 (M^+ , 9), 314 (100). UV (λ_{max} (ϵ) in 3-MP) 241.1 nm (15000). Found: C, 55.62; H, 5.20%. Calcd for $\text{C}_{20}\text{H}_{22}\text{F}_6\text{Si}_2$: C, 55.53; H, 5.13%.

1,2-Bis(*p*-methoxyphenyl)-1,2-dimethyl-1,2-disilacyclohexane (3d): Isomers were separated by preparative HPLC (hexane/AcOEt = 10/1) to give 466 mg (1.31 mmol, 44% yield) of *trans*-**3d** as colorless solids and 179 mg (0.501 mmol, 17% yield) of *cis*-**3d** as a colorless oil.

trans-**3d**: mp $72\text{--}73^\circ\text{C}$. ^1H NMR δ 0.46 (s, 6H), 1.10–1.20 (m, 4H), 1.58–1.72 (m, 2H), 1.96–2.10 (m, 2H), 3.36 (s, 6H), 6.92 (d, $J = 8.3$ Hz, 4H), 7.53 (d, $J = 8.3$ Hz, 4H). ^{13}C NMR δ –4.17, 16.24, 26.70, 54.64, 114.28, 129.04, 135.85, 160.85. ^{29}Si NMR δ –23.80. MS (EI) m/z (relative intensity) 356 (M^+ , 15), 257 (100). UV (λ_{max} (ϵ) in 3-MP) 240.0 nm (31500). Found: C, 67.50; H, 7.90%. Calcd for $\text{C}_{20}\text{H}_{28}\text{O}_2\text{Si}_2$: C, 67.36; H, 7.91%. *cis*-**3d**: ^1H NMR δ 0.48 (s, 6H), 0.98–1.07 (m, 4H), 1.22–1.31 (m, 2H), 1.76–1.91 (m, 2H), 3.30 (s, 6H), 6.84 (d, $J = 8.4$ Hz, 4H), 7.46 (d, $J = 8.4$ Hz, 4H). ^{13}C NMR δ –3.74, 16.37, 26.70, 54.56, 114.13, 128.66, 136.21, 160.81. ^{29}Si NMR δ –23.90. MS (EI) m/z (relative intensity) 356 (M^+ , 16), 257 (100). UV (λ_{max} (ϵ) in 3-MP) 237.4 nm (33900). Found: C, 67.46; H, 7.97%. Calcd for $\text{C}_{20}\text{H}_{28}\text{O}_2\text{Si}_2$: C, 67.36; H, 7.91%.

1,2-Dichloro-1,2-dimethyl-1,2-disilacyclohexane (4-Cl): To a solution of 1,2-dimethyl-1,2-diphenyl-1,2-disilacyclohexane (2.41 g, 8.13 mmol) in benzene (10 mL) was added AlCl_3 (12.1 mg, 0.0906 mmol), and then HCl gas was introduced into this mixture for 1.3 h at room temperature. Additional AlCl_3 (16.9 mg, 0.127 mmol) was added. After being stirred for 2.3 h, hexane (10 mL) and acetone (2 mL) were added to quench the reaction, and the resulting acetone/ AlCl_3 complex was removed by filtration. Evaporation followed by distillation gave 1.37 g (6.40 mmol,

79% yield) of 1,2-dichloro-1,2-dimethyl-1,2-disilacyclohexane **4-Cl** as colorless oil: bp 98–107 °C/26 mmHg (lit.^{16a} bp 102–108 °C/35 mmHg). ¹H NMR δ 0.44 (s, 6H), 0.7–0.8 (m, 2H), 1.0–1.1 (m, 2H), 1.4–1.5 (m, 2H), 1.65–1.75 (m, 2H).

1,2-Bis[*p*-(dimethylamino)phenyl]-1,2-dimethyl-1,2-disilacyclohexane (3e**):** To a mixture of 1,2-dichloro-1,2-dimethyl-1,2-disilacyclohexane **4-Cl** (652 mg, 3.06 mmol) and CuCN (29.1 mg, 0.325 mmol) in THF (6 mL) was added *p*-(dimethylamino)phenylmagnesium bromide (12.0 mmol) in THF (18 mL) dropwise for 10 min at room temperature. Upon completion of the addition, the addition funnel was rinsed with THF (2 \times 2 mL). After being stirred for 36 h, the solvent was evaporated. The residue was hydrolyzed with 10% NH₄Cl (20 mL), and Et₂O (20 mL) was added. The biphasic mixture was filtered and separated. The aqueous layer was extracted with Et₂O (4 \times 20 mL). The combined organic layer was washed with brine (40 mL) and dried over MgSO₄. After filtration and evaporation, the residue was subjected to column chromatography on silica gel (hexane/AcOEt/Et₃N = 20/1/0.6, *R_f* = 0.35). The collected fraction was subjected to preparative GPC (toluene as eluent) to give 1.13 g (2.51 mmol, 82% yield, *cis/trans* = 1/4) of **3e** as colorless solids.

Isomers were separated by silica gel column chromatography. *trans*-**3e**: colorless crystals. mp 85–86 °C. ¹H NMR δ 0.59 (s, 6H), 1.22–1.28 (m, 4H), 1.7–1.8 (m, 2H), 2.05–2.15 (m, 2H), 2.56 (s, 12H), 6.72 (d, *J* = 8.7 Hz, 4H), 7.64 (d, *J* = 8.7 Hz, 4H). ¹³C NMR δ –3.82, 16.63, 26.93, 40.06, 112.83, 123.79, 135.59, 151.17. ²⁹Si NMR δ –24.12. MS (EI) *m/z* (relative intensity) 383 (*M*⁺, 36), 283 (100). UV (λ_{\max} (ϵ) in 3-MP) 271.4 nm (45600). Found: C, 68.79; H, 8.94; N, 7.33%. Calcd for C₂₂H₃₄N₂Si₂: C, 69.05; H, 8.96; N, 7.32%. *cis*-**3e**: a colorless oil. ¹H NMR (300 MHz) δ 0.57 (s, 6H), 1.11–1.17 (m, 2H), 1.34–1.43 (m, 2H), 1.84–2.00 (m, 4H), 2.51 (s, 12H), 6.65 (d, *J* = 8.4 Hz, 4H), 7.60 (d, *J* = 8.4 Hz, 4H). ¹³C NMR (67.94 MHz) δ –3.38, 16.86, 26.90, 39.98, 112.70, 123.44, 135.98, 151.12. ²⁹Si NMR (53.67 MHz) δ –24.30. MS (EI) *m/z* (relative intensity) 383 (*M*⁺, 32), 283 (100). UV (λ_{\max} (ϵ) in 3-MP) 266.1 nm (48300). Found: C, 68.85; H, 9.03; N, 7.28%. Calcd for C₂₂H₃₄N₂Si₂: C, 69.05; H, 8.96; N, 7.32%.

Preparation of 1,1,2,2-Tetramethyl-1,2-bis(*p*-trifluoromethylphenyl)disilane (5b**). A Typical Procedure via Silyltriflate:** To a solution of 1,1,2,2-tetramethyl-1,2-diphenyldisilane **5a** (1.82 mmol) in CH₂Cl₂ (4 mL) was added TfOH (0.35 mL, 4.0 mmol) dropwise at 0 °C. After being stirred at 0 °C for 2.5 h, the solvent was evaporated. The residue was dissolved in Et₂O (4 mL) and cooled to 0 °C. To the resulting solution was added 13.0 mL (8.1 mmol) of a 0.62 M solution of *p*-(trifluoromethyl)phenylmagnesium bromide in Et₂O dropwise at 0 °C over 10 min. Upon completion of the addition, the addition funnel was rinsed with Et₂O (3 mL); then the reaction mixture was allowed to warm to room temperature. After being stirred for 14 h, the resulting mixture was hydrolyzed with 10% NH₄Cl (10 mL) and separated. The aqueous layer was extracted with Et₂O (3 \times 15 mL). The combined organic layer was washed with brine (20 mL) and dried over MgSO₄. After filtration and evaporation, the residue was distilled under reduced pressure (210 °C/33 mmHg). The fraction was subjected to short path column chromatography on silica gel (hexane, *R_f* = 0.55) to give 501 mg (1.23 mmol, 62% yield) of **5b** as colorless solids: mp 51.5–52.5 °C. ¹H NMR (300 MHz) δ 0.18 (s, 12H), 7.2 (m, 4H), 7.40 (d, *J* = 8.4 Hz, 4H). ¹³C NMR (67.94 MHz) δ –4.20, 124.54 (q, *J* = 3.7 Hz), 125.00 (q, *J* = 271.7 Hz), 130.89 (q, *J* = 32.0 Hz), 134.24, 143.70. ²⁹Si NMR (53.67

MHz) δ –20.89. MS (EI) *m/z* (relative intensity) 407 (*M*⁺, 0.7), 203 (*M*/2, 100). UV (λ_{\max} (ϵ) in 3-MP) 243.3 nm (17200). Found: C, 53.39; H, 5.02%. Calcd for C₁₈H₂₀F₆Si₂: C, 53.18; H, 4.96%.

Calculations. The initial geometry for the optimization procedure was based on the structures built on SpartanTM and performed a conformation search by MMFF. Starting with the most stable conformer, geometry optimization calculations were performed with the Gaussian 98 program with an HPC-PA264U computer at the HF/3-21G(d) level, and frequency analyses were performed at the same level, followed by MP2/6-31G(d) and then MP2/6-311G(d) level. Based on the finally optimized geometry, time-dependent (TD) density functional theory (DFT) excitation energies were calculated at the B3LYP/6-311G(d) level.

X-ray Crystallographic Analyses. Crystals of *trans*-**3d** suitable for the structural analysis were obtained by recrystallization from hexane–ethanol. A colorless crystal (0.5 \times 0.3 \times 0.1 mm³) was mounted on a cryoloop. Intensity data were collected at –100 °C on a Rigaku Saturn CCD diffractometer with graphite monochromated Mo K α radiation (λ = 0.71070 Å). The crystal structure was solved by a direct method (SIR97) and refined by a full-matrix least-square method on *F*² for all reflections (SHELX-97). All non-hydrogen atoms were refined anisotopically. All hydrogen atoms were placed using AFIX instructions and refined isotopically. The crystal data and analytical conditions are summarized in Table 1.

Crystallographic data have been deposited with Cambridge Crystallographic Data Centre: Deposition number CCDC-266593 for *trans*-**3d**. Copies of the data can be obtained free of charge via <http://www.ccdc.cam.ac.uk/conts/retrieving.html> (or from the Cambridge Crystallographic Data Centre, 12, Union Road, Cambridge, CB2 1EZ, UK; Fax: +44 1223 336033; e-mail: deposit@ccdc.cam.ac.uk).

Financial support by the Ministry of Education, Culture, Sports, Science and Technology, Japan, for the Grant-in-Aid for COE Research on Elements Science, No. 12CE2005 for K. T. and Kinki Invention Center for H. T. are gratefully acknowledged.

References

- # Some preliminary results of the present work were obtained by T. T. in the Kumada Laboratory in 1972, at the Department of Synthetic Chemistry, Faculty of Engineering, Kyoto University.
- 1 a) C. G. Pitt, M. M. Bursey, and P. F. Rogerson, *J. Am. Chem. Soc.*, **92**, 519 (1970). b) H. Bock and W. Ensslin, *Angew. Chem., Int. Ed. Engl.*, **10**, 404 (1971). c) K. Mochida, S. D. Worley, and J. K. Kochi, *Bull. Chem. Soc. Jpn.*, **58**, 3389 (1985). d) D. L. Casher, H. Tsuji, A. Sano, M. Katkevics, A. Toshimitsu, K. Tamao, M. Kubota, T. Kobayashi, H. Ottosson, D. E. David, and J. Michl, *J. Phys. Chem. A*, **107**, 3559 (2003).
- 2 a) H. Bock and H. Alt, *J. Am. Chem. Soc.*, **92**, 1569 (1970). b) C. G. Pitt and H. Bock, *J. Chem. Soc., Chem. Commun.*, **1972**, 28.
- 3 a) H. Gilman, W. H. Atwell, and G. L. Schwebke, *Chem. Ind. (London)*, **1964**, 1063. b) H. Gilman, W. H. Atwell, and G. L. Schwebke, *J. Organomet. Chem.*, **2**, 369 (1964). c) H. Sakurai and M. Kumada, *Bull. Chem. Soc. Jpn.*, **37**, 1894 (1964). d) D. N. Hague and R. H. Prince, *Chem. Ind. (London)*, **1964**, 1492.
- 4 For reviews see: a) M. Kumada and K. Tamao, *Adv. Orga-*

- nomet. Chem.*, **6**, 19 (1968). b) R. D. Miller and J. Michl, *Chem. Rev.*, **89**, 1359 (1989). c) R. West, "Comprehensive Organometallic Chemistry II," ed by E. W. Abel, F. G. A. Stone, and G. Wilkinson, Pergamon, Oxford (1995), p. 77. d) J. Michl and R. West, "Silicon-Containing Polymers," ed by R. G. Jones, W. Ando, and J. Chojnowski, Kulwer Academic Publishers, Dordrecht (2000), p. 499. e) R. West, "The Chemistry of Organosilicon Compounds," ed by Z. Rappoport and Y. Apeloig, Wiley, Chichester (2001), Vol. 3, p. 541. f) H. Tsuji, J. Michl, and K. Tamao, *J. Organomet. Chem.*, **685**, 9 (2003).
- 5 G. C. Pitt, R. N. Carey, and E. C. Toren, *J. Am. Chem. Soc.*, **94**, 3806 (1972).
- 6 Reviews see: a) H. Sakurai, *J. Organomet. Chem.*, **200**, 261 (1980). b) H. Sakurai, *Pure Appl. Chem.*, **59**, 1637 (1987).
- 7 For example: J. Oshita, *J. Synth. Org. Chem. Jpn.*, **59**, 13 (2001).
- 8 a) H. Sakurai, S. Tasaka, and M. Kira, *J. Am. Chem. Soc.*, **94**, 9285 (1972). b) M. Kira, T. Miyazawa, N. Mikami, and J. Sakurai, *Organometallics*, **10**, 3793 (1991).
- 9 For reviews see: a) A. G. Brook, "The Chemistry of Organosilicon Compounds, Part 2," ed by S. Patai and Z. Rappoport, Wiley, Chichester (1989), p. 965. b) M. Kira and T. Miyazawa, "The Chemistry of Organosilicon Compounds," ed by Z. Rappoport and Y. Apeloig, Wiley, Chichester (1998), Vol. 2, p. 1311. c) A. G. Brook, "The Chemistry of Organosilicon Compounds," ed by Z. Rappoport and Y. Apeloig, Wiley, Chichester (1998), Vol. 2, p. 1233.
- 10 K. Tamao, M. Kumada, and M. Ishikawa, *J. Organomet. Chem.*, **31**, 17 (1971).
- 11 Review: H. Tsuji, J. Michl, A. Toshimitsu, and K. Tamao, *J. Synth. Org. Chem. Jpn.*, **60**, 762 (2002).
- 12 a) K. Tamao, H. Tsuji, M. Terada, M. Asahara, S. Yamaguchi, and A. Toshimitsu, *Angew. Chem., Int. Ed.*, **39**, 3287 (2000). b) H. Tsuji, A. Toshimitsu, K. Tamao, and J. Michl, *J. Phys. Chem. A*, **105**, 10246 (2001). c) H. A. Fogarty, H. Tsuji, D. E. David, C. H. Ottosson, M. Ehara, H. Nakatsuji, K. Tamao, and J. Michl, *J. Phys. Chem. A*, **106**, 2369 (2002). d) H. Tsuji, M. Terada, A. Toshimitsu, and K. Tamao, *J. Am. Chem. Soc.*, **125**, 7486 (2003). e) S. Seki, K. Okamoto, Y. Matsui, S. Tagawa, H. Tsuji, A. Toshimitsu, and K. Tamao, *Chem. Phys. Lett.*, **380**, 141 (2003). f) H. Mallesha, H. Tsuji, and K. Tamao, *Organometallics*, **23**, 1639 (2004). g) H. Tsuji, A. Fukazawa, S. Yamaguchi, A. Toshimitsu, and K. Tamao, *Organometallics*, **23**, 3375 (2004).
- 13 a) H. Sakurai, H. Yamamori, and M. Kumada, *Bull. Chem. Soc. Jpn.*, **38**, 2024 (1965). b) H. Kelling, *Z. Chem.*, **7**, 237 (1967).
- c) H. Gilman and P. J. Morris, *J. Organomet. Chem.*, **6**, 102 (1966). d) A. Hosomi and H. Sakurai, *Chem. Lett.*, **1972**, 193.
- 14 W. Uhlig, *Chem. Ber.*, **129**, 733 (1996).
- 15 a) P. J. Lennon, D. P. Mack, and Q. E. Thompson, *Organometallics*, **8**, 1121 (1989). b) K. Tamao, H. Tsuji, and A. Toshimitsu, *Synlett*, **2000**, 964.
- 16 a) K. Tamao, M. Kumada, and M. Ishikawa, *J. Organomet. Chem.*, **31**, 35 (1971). b) M. Ishikawa, S. Shirai, A. Naka, H. Kobayashi, J. Ohshita, A. Kunai, Y. Yamamoto, S.-H. Cha, K. Lee, and Y.-W. Kwak, *Organometallics*, **21**, 4206 (2002).
- 17 This is similar to the proposed geometry for the pyrene-substituted disilane. D. Declercq, P. Delbeke, F. C. De Schryver, L. Van Meervelt, and R. D. Miller, *J. Am. Chem. Soc.*, **115**, 5702 (1993).
- 18 The π^* (SiSi) orbital comprises the in-phase overlap of the SiC_3 group orbitals. See Ref. 1d.
- 19 H. Hiratsuka, Y. Mori, M. Ishikawa, K. Okazaki, and H. Shizuka, *J. Chem. Soc., Faraday Trans. 2*, **81**, 1665 (1985).
- 20 G. H. Weeks, W. Adcock, K. A. Klingensmith, J. W. Waluk, R. West, M. Vasak, J. Downing, and J. Michl, *Pure Appl. Chem.*, **58**, 39 (1986).
- 21 a) H. Shizuka, H. Obuchi, M. Ishikawa, and M. Kumada, *J. Chem. Soc., Chem. Commun.*, **1981**, 405. b) M. Ishikawa, H. Sugisawa, T. Fuchikami, M. Kumada, T. Manabe, H. Kawakami, K. Fukui, Y. Ueki, and H. Shizuka, *J. Am. Chem. Soc.*, **104**, 2872 (1982). c) H. Shizuka, Y. Sato, M. Ishikawa, and M. Kumada, *J. Chem. Soc., Chem. Commun.*, **1982**, 439. d) H. Shizuka, Y. Sato, Y. Ueki, M. Ishikawa, and M. Kumada, *J. Chem. Soc., Faraday Trans. 1*, **80**, 341 (1984). e) H. Shizuka, H. Obuchi, M. Ishikawa, and M. Kumada, *J. Chem. Soc., Faraday Trans. 1*, **80**, 383 (1984). f) H. Shizuka, K. Okazaki, M. Tanaka, M. Ishikawa, M. Sumitani, and K. Yoshihara, *Chem. Phys. Lett.*, **113**, 89 (1985). g) M. Yamamoto, T. Kudo, M. Ishikawa, S. Tobita, and H. Shizuka, *J. Phys. Chem. A*, **103**, 3144 (1999).
- 22 a) H. Sakurai, H. Sugiyama, and M. Kira, *J. Phys. Chem.*, **94**, 1837 (1990). b) M. Kira, T. Miyazawa, H. Sugiyama, M. Yamaguchi, and H. Sakurai, *J. Am. Chem. Soc.*, **115**, 3116 (1993). c) Y. Tajima, H. Ishikawa, T. Miyazawa, M. Kira, and N. Mikami, *J. Am. Chem. Soc.*, **119**, 7400 (1997). d) H. Ishikawa, Y. Shimanuki, M. Sugiyama, Y. Tajima, M. Kira, and N. Mikami, *J. Am. Chem. Soc.*, **124**, 6220 (2002). e) H. Ishikawa, M. Sugiyama, T. Kishi, M. Kira, N. Mikami, O. Kajimoto, and A. Mahipal Reddy, *Chem. Phys.*, **283**, 379 (2002).
- 23 D. F. Eaton, *Pure Appl. Chem.*, **60**, 1107 (1988).